Applied Catalysis B: Environmental 211 (2017) 199–204

Contents lists available at ScienceDirect

Applied Catalysis B: Environmental

journal homepage: www.elsevier.com/locate/apcatb

Photocatalytic performance enhancement of CuO/Cu_2O heterostructures for photodegradation of organic dyes: Effects of CuO morphology

Denghui Jiang[a], Jianbin Xue[a,c], Liqiong Wu[a], Wei Zhou[a], Yuegang Zhang[b], Xinheng Li[a,*]

[a] The State Key Laboratory for Oxo Synthesis and Selective Oxidation, Suzhou Research Institute of LICP, Lanzhou Institute of Chemical Physics (LICP), Chinese Academy of Sciences, Suzhou 215123, China
[b] i-Lab, Suzhou Institute of Nano-tech and Nano-bionics, Chinese Academy of Sciences, Suzhou 215123, China
[c] University of Chinese Academy of Sciences, Beijing 100049, China

ARTICLE INFO

Article history:
Received 10 February 2017
Received in revised form 26 March 2017
Accepted 9 April 2017
Available online 13 April 2017

Keywords:
Heterostructures
Cu2O
Morphology
Nanostructures

ABSTRACT

Cuprous oxide is a promising candidate for photocatalysis. But its photocatalytic properties still need to be much improved for applications. Herein, we report a kind of heterostructures (HCs), i.e. CuO/Cu_2O HCs. Different morphologies of CuO, i.e. nanowires, nanotetrahedra and nanospheres, have been controllably prepared on Cu_2O cubes/octahedra by a facile wet chemical method. All the obtained CuO/Cu_2O HCs have significantly improved photocatalytic activity and stability as compared to Cu_2O. Especially, the nanowires CuO/Cu_2O have shown a specific reaction rate ca. 1.6 $\mu mol\ min^{-1}\ g^{-1}$, 260 times as high as pristine Cu_2O and 4 times as Au/Cu_2O. And the nanospheres CuO/Cu_2O have maintained over 95% of photocatalytic activity after 7 cycles. So, distinct morphologies of CuO have resulted in dramatic effects on photocatalytic properties of CuO/Cu_2O HCs.

1. Introduction

Photocatalytic materials have promising applications in environmental remediation. But they have to meet high requirements, i.e. visible light absorption, good charge separation, available reaction sites accessibility and earth-abundance as well as environment benignity [1–4]. Since synthesis of Cu_2O with well-defined morphologies has become controllable, cuprous oxide has attracted great attentions for photocatalysis due to its non-toxicity and earth-abundance [5]. However, photocatalytic activity and stability of Cu_2O still need to be much improved. Aiming for solving the above problems, several strategies have been taken to enhance photocatalytic performances of Cu_2O.

One strategy is to form heterostructures (HCs) by combining cocatalysts like metal oxides, r-GO etc [6,7]. Take a few for examples. Core–shell TiO_2/Cu_2O [8,9], α-Fe_2O_3/Cu_2O [10], sandwich-structured $Cu/Cu_2O/CuO$ as photocathodes [11], and Fe_xO_y nanosheets/Cu_2O cubes [12]. have been reported. Those HCs showed better photocatalytic activities than Cu_2O alone. Very recently, molecular catalyst as a cocatalyst has also been reported [13]. Grätzel reported immobilization of a molecular catalyst on Cu_2O as photocathode for CO_2 reduction, which effectively enhanced photocatalytic reduction efficiency. The other strategy is to assemble cubic and rhombic dodecahedral Cu_2O and the ensembles showed enhanced optoelectronic properties as compared to disordered Cu_2O [14]. Another strategy is plasmonic nano-metals enhancement of Cu_2O photocatalytic activity [15–17]. Au/Cu_2O and Ag/Cu_2O demonstrated superior photocatalytic performances.

Based on energy band theory, CuO and Cu_2O also can form HCs with a type II structure, which facilitates charge separation improving photocatalytic activity. But to prepare such allotropic CuO/Cu_2O HCs has been rarely investigated, to the best of our knowledge. Herein, we report controllable preparation of CuO/Cu_2O HCs and explore the HCs enhance photocatalytic properties. Different morphologies of CuO, i.e. nanowires (NW), tetrahedra (TH), and nanospheres (NS), have been controllably prepared on Cu_2O cubes/octahedra. Enhancements of photocatalytic activity and stability by distinct morphologies of CuO/Cu_2O HCs have been investigated. By comparison, the effect of CuO morphology on photocatalytic activity and stability of CuO/Cu_2O HCs was studied. Based on the above studies, possible photocatalytic mechanism and HCs formation mechanism were hypothesized.

* Corresponding author.
E-mail address: xinhengli@licp.cas.cn (X. Li).

http://dx.doi.org/10.1016/j.apcatb.2017.04.034
0926-3373/

2. Experimental

2.1. Synthesis of Cu_2O cubes and octahedra

All of the chemical reagents used in this experiment were analytical grade and used without further purification. Cu_2O cubes and octahedra were prepared according to a previously reported method [15]. In a typical procedure, 5 mL of 200 mM NaOH aqueous solution was added dropwisely to 50 mL of 0.01 M $CuCl_2$ aqueous solution at 55 °C. For preparation of octahedral Cu_2O, 1.667 g polyvinylpyrrolidone (PVP, MW = 55,000) was added. After stirring for 0.5 h, 5 mL of 0.6 M ascorbic acid aqueous solution was added dropwisely to the above solution. The mixed solution was kept at 55 °C with vigorous stirring for a certain time (cubes for 5 h, octahedra for 3 h). Finally, the mixed solution gradually became brick-red, indicating formation of Cu_2O. The obtained products were washed with DI water and absolute ethanol several times, and dried in a vacuum oven at 40 °C for 6 h.

2.2. Synthesis of CuO/Cu_2O HCs

2.2.1. NW CuO/Cu_2O

Typical NW CuO/Cu_2O sample was synthesized as follows. A 43.3 mg sample of Cu_2O cubes or octahedra was added to 10 mL of 200 mM NaOH aqueous solution with ultrasonication. And then, the mixed solution was magnetically stirred at room temperature (RT) for 3 h. The as-obtained product was collected by centrifugation, washed with distilled water and absolute ethanol several times. Finally, the product was dried in a vacuum oven at 40 °C for 6 h.

2.2.2. TH CuO/Cu_2O

Typical TH CuO/Cu_2O sample was synthesized as follows. A quantity of 43.3 mg of Cu_2O cubes was added to 5 mL of 0.2 M NaCl or $NaNO_3$ aqueous solution with ultrasonication. And then, the suspension solution was reacted at room temperature for 5 h. After the reaction, the product was collected by centrifugation, washed with DI water and absolute ethanol for several times respectively. Finally, the product was dried in a vacuum oven at 40 °C for 6 h.

2.2.3. NS CuO/Cu_2O

Typical NS CuO/Cu_2O sample was synthesized as follows. A quantity of 43.3 mg of Cu_2O cubes was added to 30 mL of 100 mM EDA aqueous solution with ultrasonication. And then, the suspension solution was sealed into an autoclave vessel and heated at 180 °C for 5 h. After the reaction, the product was collected by centrifugation, washed with DI water and absolute ethanol for several times respectively. Finally, the product was dried in a vacuum oven at 40 °C for 6 h.

2.2.4. Au/Cu_2O

Au/Cu_2O cubes sample was prepared according to our previously reported method [15]. Typical procedure is as follows. 20 mg Cu_2O cubes sample was dispersed into 3 mL distilled water by ultrasonication. And then the suspension was irradiated under a 300 W Xe lamp (PLS-SXE300). Under continuous stirring, 2.0 mL of 0.0625 g/L $HAuCl_4$ aqueous solution was added to the above suspension, and the suspension was further irradiated for 1 h. After that, the products were collected by centrifugation, washed with distilled water and absolute ethanol several times, and dried in a vacuum oven at 40 °C for 6 h.

2.2.5. Control experiment: oxidation of Cu_2O cubes in air

60 mg of Cu_2O cubes was heated up to 400 °C in air at a rate of 5 °C min^{-1} and kept at 400 °C for 1 h before it was allowed to cool down to room temperature.

2.3. Characterizations

The X-ray diffraction(XRD) patterns of the products were measured by using a Bruker D8 Discover diffractometer with Cu-K_α radiation (λ = 0.15406 nm) at a scanning rate of 0.02 deg/s in a 2θ range from 20 to 80°. Scanning electron microscopy (SEM) images were obtained using a Hitachi S4800 scanning electron microscopy. Transmission electron microscopy (TEM) images were recorded on a FEI Tecnai G2 F20 S-TWIN microscope operating at 200 kV. Elemental analysis of the samples was conducted using an energy-dispersive X-ray analysis system attached to the TEM. UV–vis absorption spectra were recorded on a PE Lambda 650 s UV–vis spectrometer. X-ray photoelectron spectra were recorded on a Escalab 250 Xi X-ray photoelectron spectroscopy (XPS).

2.4. Photocatalytic activity and stability tests

Photocatalytic tests were carried out as follows. 15 mg of photocatalyst sample was dispersed into 50 mL of 2×10^{-5} M methyl orange (MO) aqueous solution. The suspended solution was magnetically stirred in the darkness for 0.5 h to reach an adsorption/desorption equilibrium. And then, the mixed solution was irradiated under a 300 W Xe lamp (PLS-SXE300, 150 mw/cm^2) equipped with UV filter (cutoff wavelength λ = 420 nm) from a distance of ca. 15 cm. At a given time interval, 1 mL aliquot of the mixed solution was taken out and centrifuged. And then photocatalytic activity was tested according to absorption spectra of MO, recorded on a UV–vis absorption spectrophotometer (PE Lambda 650s).

3. Results and discussion

3.1. NW CuO/Cu_2O

Fig. 1 shows SEM, TEM images and XRD patterns of NW CuO/Cu_2O made by mild etching of 200 mM NaOH aqueous solution. Morphology and optical property of Cu_2O cubes are shown in Fig. S1. Cu_2O cubes with an edge length ca. 585 nm show good monodispersity. UV–vis absorption spectrum of Cu_2O shows a peak at λ = 484 nm attributed to band absorption and a peak at λ = 550 nm attributed to scattering [18]. In Fig. 1, CuO exhibits nanowire morphology with a diameter of ca. 60 nm and a length of a couple of micrometers. The CuO NWs lie down on the surfaces of Cu_2O cubes. The lattice spacing of 0.232 nm in high resolution TEM (HRTEM) image is assigned to (111) plane of CuO. So, HRTEM image and selective area electron diffraction (SAED) pattern prove the nanowires are CuO and crystalline. Our XPS results in Fig. S2 also show the formation of CuO on surface, in good agreement with HRTEM images. X-ray diffraction (XRD) patterns of the obtained CuO/Cu_2O further demonstrate CuO NWs and Cu_2O in HCs are crystalline. In order to prove feasibility of this method, we did a series of experiments and found surface density of CuO NWs increased with increasing concentration of NaOH aqueous solution, as shown in Fig. S3. CuO morphology changed from nanoflakes to nanowires to flower-like assemblies with the increase of NaOH concentration, clearly indicating NW CuO crystal growth process. FTIR spectra of the samples obtained at different reaction time show intermediate $Cu(OH)_2$ formed and its peak intensity decreased as the reaction time elapsed, as shown in Fig. S4. This is in good agreement with an earlier literature, where Cu_2O reacted with NaOH aqueous solution to form $Cu(OH)_2$ nanowires [19]. Also, this suggests transition from $Cu(OH)_2$ to CuO since $Cu(OH)_2$ easily turns into CuO upon exposed to air and drying.

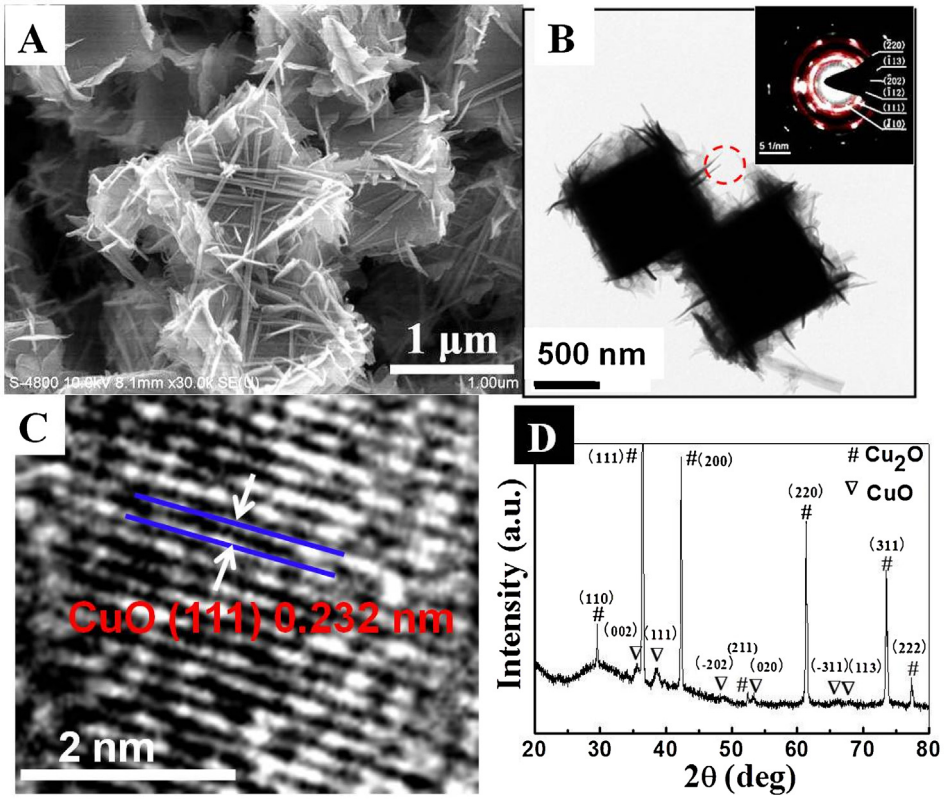

Fig. 1. SEM image (A), TEM image (B), HRTEM image (C), and XRD spectrum (D) of NW CuO/Cu_2O under 200 mM of NaOH aqueous solution condition. Inset image is electron diffraction patterns of the as-obtained NW CuO/Cu_2O sample. The lattice spacing 0.232 nm is attributed to (111) plane of CuO. XRD patterns show formed CuO is crystalline.

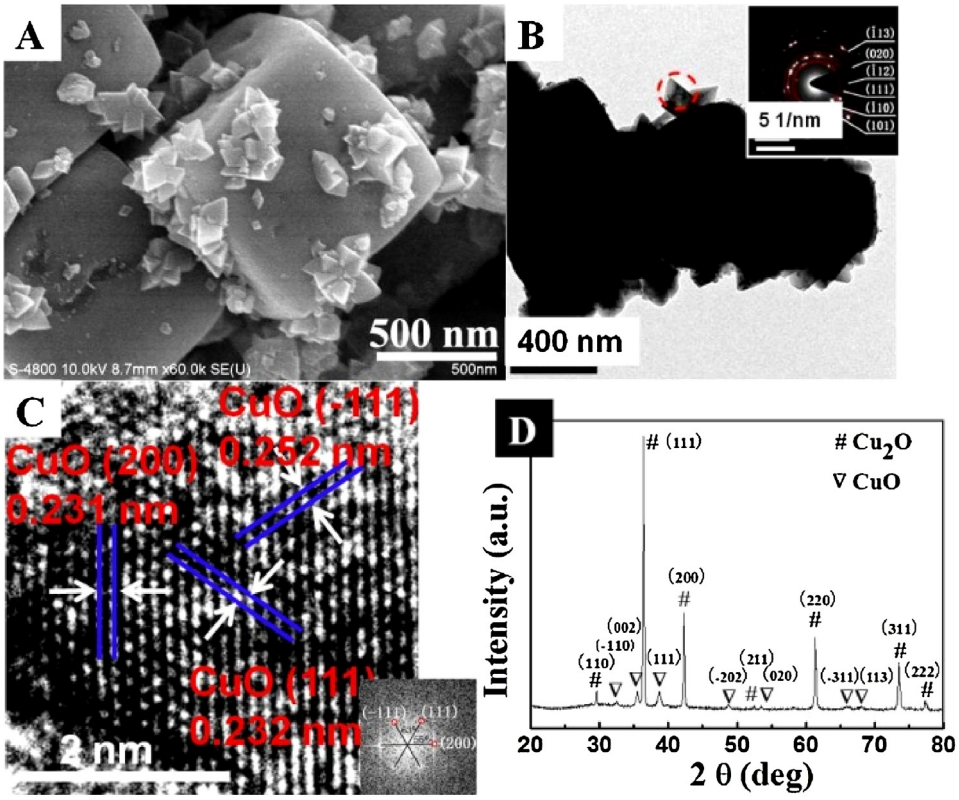

Fig. 2. SEM image (A), TEM image (B), HRTEM image (C), and XRD spectrum (D) of TH CuO/Cu_2O under 200 mM of NaCl aqueous solution condition. Inset image is electron diffraction pattern of the as-obtained TH CuO/Cu_2O sample. The lattice spacings of 0.232 nm, 0.231 nm and 0.252 nm are attributed to (111), (200), (-111) planes of CuO respectively. XRD patterns show coexistence of CuO and Cu_2O and both of them are crystalline.

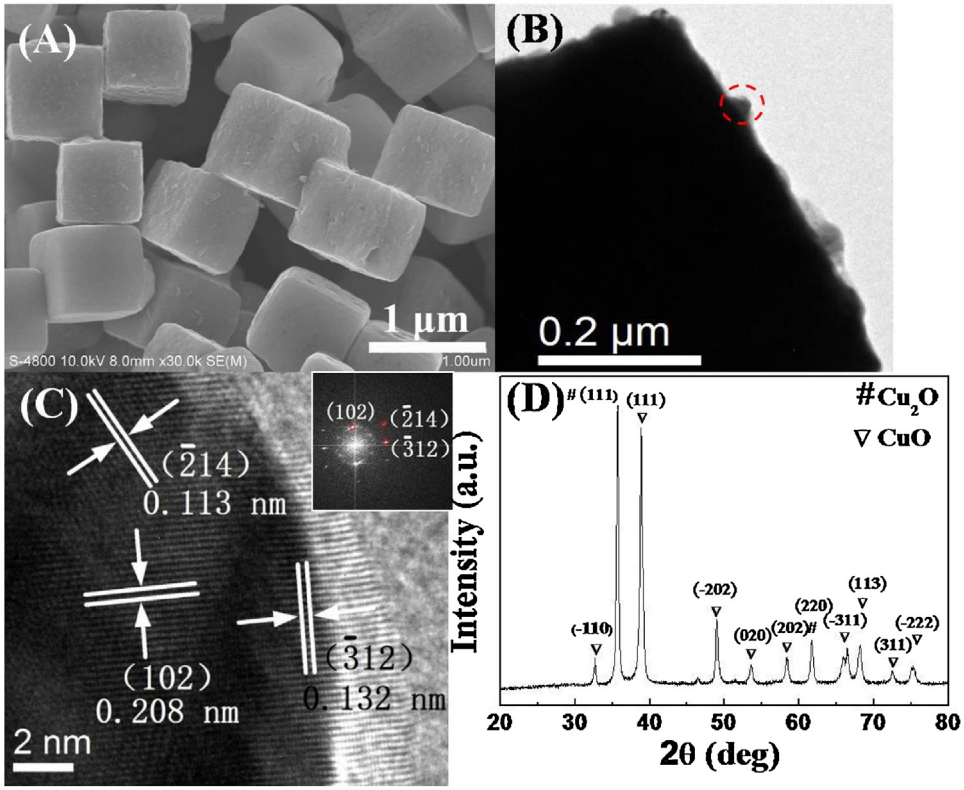

Fig. 3. SEM image (A), TEM image (B), HRTEM image (C), and XRD spectrum (D) of NS CuO/Cu_2O under hydrothermal condition with 100 mM of EDA aqueous solution condition. Inset image is FFT electron diffraction pattern of the as-obtained NS CuO/Cu_2O sample. The lattice spacings of 0.208 nm, 0.132 nm and 0.113 nm are attributed to (102), (312), (214) planes of CuO respectively. XRD patterns show coexistence of CuO and Cu_2O and both of them are crystalline.

3.2. *TH CuO/Cu_2O and NS CuO/Cu_2O*

Fig. 2 is SEM, TEM images and XRD patterns of TH CuO/Cu_2O. TH CuO/Cu_2O were made by adding NaCl aqueous solution at room temperature. The SEM image shows formation of TH CuO on Cu_2O cubes, which lie on the surfaces, edges, and corners of Cu_2O cubes and mostly form aggregates. The edge length of the TH CuO is ca. 125 ± 54 nm. The lattice spacings of 0.232 nm, 0.252 nm and 0.231 nm in HRTEM image are assigned to(111)and(-111)and (200) planes of CuO respectively. So, HRTEM images and SAED pattern verify tetrahedral objects are CuO and crystalline. XRD patterns of the as-obtained CuO/Cu_2O further prove tetrahedral CuO and Cu_2O are crystalline. Moreover, we used octahedral Cu_2O other than cubes and found similar tendency. This is to say that tetrahedral CuO also formed on octahedral Cu_2O, as shown in Fig. S5. This shows TH CuO can form on both (111) and (100) facets.

Fig. 3 is SEM, TEM images and XRD patterns of NS CuO/Cu_2O. NS CuO/Cu_2O were prepared in 100 mM EDA aqueous solution under hydrothermal treatment. The diameter of CuO nanospheres is ca. 48 ± 25 nm. The lattice spacings of 0.208 nm, 0.113 nm and 0.132 nm in HRTEM image are attributed to (102), (214) and (312) planes of CuO respectively. So, HRTEM images and FFT diffraction patterns prove the nanospheres are CuO and crystalline. XRD patterns of the as-obtained NS CuO/Cu_2O further corroborate spherical CuO and Cu_2O are crystalline.

3.3. *Improved photocatalytic activity and stability of CuO/Cu_2O HCs*

Photocatalytic activity and stability of the as-obtained CuO/Cu_2O HCs were tested by photocatalytic degradation of methyl orange (MO) as a model reaction, as shown in Figs. 4 and 5. It is unambiguous that all the obtained HCs have significantly improved photocatalytic activity and stability as compared to Cu_2O. Specifically, the NW CuO/Cu_2O photodegraded more than 90% of MO in ca. 30 min while Cu_2O cubes photodegraded less than 10% in 120 min. In order to exclude the effect of surface area, we measured BET specific surface areas of the as-obtained CuO/Cu_2O HCs and Cu_2O cubes shown in Table 1 of Supplementary material. Calculated reaction rate per surface area of NW CuO/Cu_2O still kept a much higher value than that of Cu_2O. Additionally, we did ultra-long time dark adsorption test for 2.5 h shown in Fig. S6A and the results showed no considerable change on adsorption of organic dyes. So, we think slightly increased surface area would not result in considerable effect on photocatalytic activity. Regarding photocatalytic activity of CuO, we did control experiments shown in Fig. S7, where Cu_2O cubes got oxidized at elevated temperatures ranging from 100 °C to 400 °C in air. Indeed, neither partially oxidized nor fully oxidized Cu_2O had noticeable photocatalytic activity. So, the enhancement of photocatalytic activity should come from formation of CuO/Cu_2O HCs. It is needed to note the enhancement of photocatalytic activity is subject to CuO loading amount, as shown in Fig. S6B. This is to say much higher/lower loading of CuO resulted in lower reaction rates, suggesting reaction site is not CuO but Cu_2O. In the meanwhile, TH and NS CuO/Cu_2O also enhanced greatly photocatalytic activities of Cu_2O, as shown in Fig. 4B and C. Both of them showed a similar trend, i.e. only moderate loading amount of CuO resulted in a maximal enhancement factor. These findings further verify reaction sites were Cu_2O instead of CuO.

In Fig. 5, NW CuO/Cu_2O and TH CuO/Cu_2O maintained over 94% of photocatalytic activity after 4 cycles. Interestingly, NS CuO/Cu_2O maintained over 95% of photocatalytic activity after seven cycles. After the stability test, NS CuO/Cu_2O still maintained good shape,

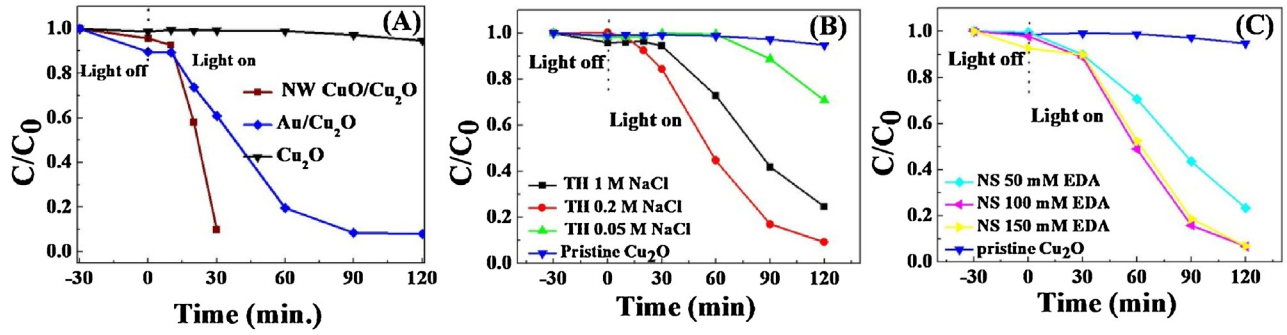

Fig. 4. Photo-degradation activities of MO by NW CuO/Cu_2O (A) as compared to pristine CuO and Au/CuO, TH CuO/Cu_2O with different loading amounts of CuO (B), and NS CuO/Cu_2O with different loading amounts of CuO (C).

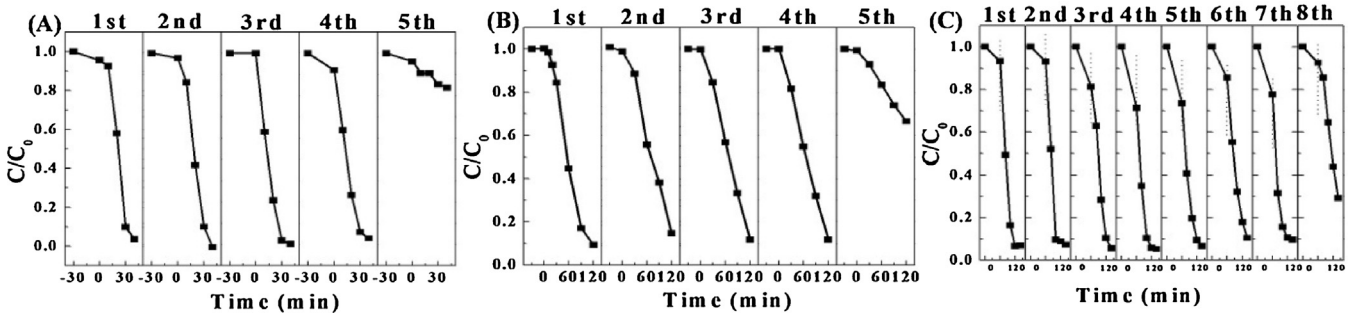

Fig. 5. Photocatalytic stability tests of NW CuO/Cu_2O (A), TH CuO/Cu_2O (B), and NS CuO/Cu_2O (C).

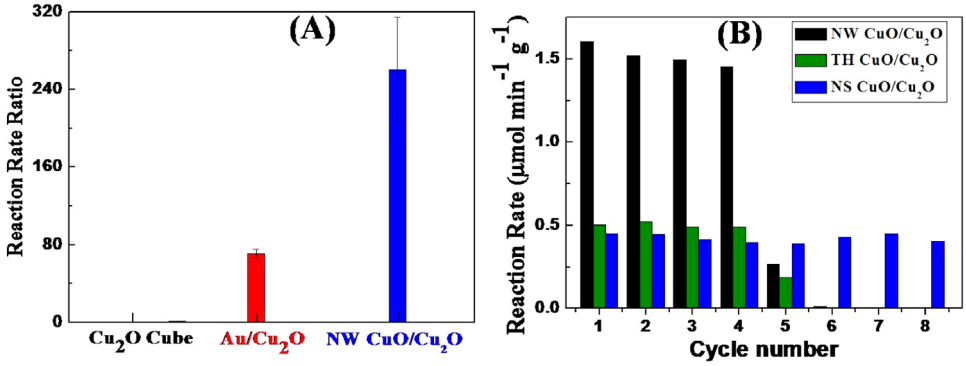

Fig. 6. Photocatalytic reaction rate ratio of NW CuO/Cu_2O and Au/Cu_2O as compared to pristine Cu_2O cubes (A), reaction rates of NW, TH and NS CuO/Cu_2O as a function of cycle number (B).

though Cu_2O surface became roughened, as shown in Fig. S8. Both NW and TH CuO/Cu_2O turned into similar morphology, where cubic morphology was not clear as NS CuO/Cu_2O. The SEM observations are in good agreement with our photocatalytic stability tests. Hence, all the CuO/Cu_2O HCs significantly enhanced photocatalytic stability of Cu_2O.

Fig. 6A summarizes photocatalytic reaction rates of NW CuO/Cu_2O and Au/Cu_2O and Cu_2O. NW CuO/Cu_2O has shown a specific reaction rate ca. 1.6 μmol min^{-1} g^{-1}, 260 times as high as pristine Cu_2O and 4 times as Au/Cu_2O [15]. The reasons for choosing Au/Cu_2O for comparison are: (1) Au/Cu_2O HC is well reproducible; (2) Au has shown great enhancement on Cu_2O photocatalytic activity due to surface plasmon resonance effect. According to enhancement factor of photocatalytic activity, the order is NW > TH > NS. Fig. 6B shows reaction rates of all three CuO/Cu_2O HCs as a function of cycle number, where NS demonstrated the best stability.

3.4. Possible photocatalytic mechanism and HCs formation mechanism

CuO is a p-type semiconductor with a narrow band gap of 1.3–1.6 eV [20]. Its conduction band and valence band are lower than the corresponding bands of Cu_2O [21]. So, CuO/Cu_2O HCs formed a type II staggered band structure and favored charge transfer resulting in improved photocatalytic activities, as shown in Fig. S9. In general, charge separation rate at the interface of the same heterostructure is dependent on contact area. With similar loading amount of CuO, NW lying down on the surface should have had biggest contact area while TH just had one facet and NS had less than half in contact respectively. Moreover, NW must have had larger surface area than TH and NS based on the same mass, which would facilitate surface adsorption and charge transport. Regarding the photocatalytic activity difference between TH and NS, the reason is the loading amount of TH CuO was slightly larger than that of NS CuO, as shown in Figs. 2 and 3.

In terms of formation of CuO with distinct morphologies, it is known that Cu_2O in NaOH aqueous solution can form $Cu(OH)_2$ nanowires [19] and copper precursor with halide precursor tends to form CuCl and CuBr dendrites [22,23]. Hence, we hypothesize different intermediates, i.e. $Cu(OH)_2$, CuCl and Cu(EDA)x, were formed. And those intermediates had different chemical affinity to Cu_2O and inherent growth orientation leading to different morphologies consequently.

4. Conclusions

In conclusion, we have investigated a kind of Cu_2O heterostructures, i.e. CuO/Cu_2O HCs. Different morphologies of CuO have been controllably formed on Cu_2O by a facile chemical method. Nanowires, nanotetrahedra, nanospheres of CuO were respectively formed on Cu_2O surfaces. All the obtained HCs have significantly improved photocatalytic activity and stability as compared to Cu_2O. Especially, the nanowires CuO/Cu_2O have shown a specific reaction rate ca. 1.6 $\mu mol\ min^{-1}\ g^{-1}$, 260 times as high as pristine Cu_2O and 4 times as Au/Cu_2O. And the nanospheres CuO/Cu_2O have maintained over 95% of photocatalytic activity after 7 cycles. So, distinct morphologies of CuO have resulted in dramatic effects on photocatalytic properties of CuO/Cu_2O HCs. The reasons for photocatalytic activity enhancements are mainly the result of formation of a type II band structure favoring charge separation and transfer. This study would provide a way to exploiting uses of earth-abundant metal oxides aiming for improving photocatalytic performance.

Acknowledgements

X.-H. Li Acknowledges financial support from National Natural Science Foundation of China (No. 21573263), National Key Research and Development Program of China from Ministry of Science and Technology of China (No. 2016YFE0105700), Jiangsu Provincial Fundamental Research Foundation of China (No. BK20151236), and Henan Provincial Open and Cooperation Foundation of China (No. 6). D.-H. Jiang is grateful for financial support from National Natural Science Foundation of China (No. 51402346).

Appendix A. Supplementary data

Supplementary data associated with this article can be found, in the online version, at http://dx.doi.org/10.1016/j.apcatb.2017.04.034.

References

[1] C.W. Tan, G.Q. Zhu, M. Hojamberdiev, K. Okada, J. Liang, X.C. Luo, P. Liu, Co_3O_4 nanoparticles-loaded BiOCl nanoplates with the dominant {001} facets: efficient photodegradation of organic dyes under visible light, Appl. Catal. B: Environ. 152–153 (2014) 425–436.
[2] J.G. Hou, C. Yang, Z. Wang, Q.H. Ji, Y.T. Li, G.C. Huang, S.Q. Jiao, H.M. Zhu, Three-dimensional Z-scheme AgCl/Ag/-TaON heterostructural hollow spheres for enhanced visible-light photocatalytic performance, Appl. Catal. B: Environ. 142–143 (2013) 579–589.
[3] Y. Gai, J. Li, S.S. Li, J.B. Xia, S.-H. Wei, Design of narrow-gap TiO_2: a passivated codoping approach for enhanced photoelectrochemical activity, Phys. Rev. Lett. 102 (2009) 036402.
[4] F. Han, V.S.R. Kambala, M. Srinivasan, D. Rajarathnam, R. Naidu, Tailored titanium dioxide photocatalysts for the degradation of organic dyes in wastewater treatment: a review, Appl. Catal. A 359 (2009) 25–40.
[5] W.-C. Huang, L.-M. Lyu, Y.-C. Yang, M.H. Huang, Synthesis of Cu_2O nanocrystals from cubic to rhombic dodecahedral structures and their comparative photocatalytic activity, J. Am. Chem. Soc. 134 (2012) 1261–1267.
[6] S. Deng, V. Tjoa, H.-M. Fan, H.-R. Tan, D.C. Sayle, M. Olivo, S. Mhaisalkar, J. Wei, C.H. Sow, Reduced graphene oxide conjugated Cu_2O nanowire mesocrystals for high-performance NO_2 gas sensor, J. Am. Chem. Soc. 134 (2012) 4905–4917.
[7] P. Dai, W. Li, J. Xie, Y. He, J. Thorne, G. McMahon, J. Zhan, D. Wang, Forming buried junctions to enhance the photovoltage generated by cuprous oxide in aqueous solutions, Angew. Chem. Int. Ed. 53 (2014) 13493–13497.
[8] L. Liu, W. Yang, Q. Li, S. Gao, J.K. Shang, Synthesis of Cu_2O nanospheres decorated with TiO_2 nanoislands, their enhanced photoactivity and stability under visible light illumination, and their post-illumination catalytic memory, ACS Appl. Mater. Interfaces 6 (2014) 5629–5639.
[9] L. Liu, W. Yang, W. Sun, Q. Li, J.K. Shang, Efficient visible-light photocatalytic hydrogen evolution and enhanced photostability of core@shell Cu_2O@g-C_3N_4 octahedra, ACS Appl. Mater. Interfaces 7 (2015) 1465–1476.
[10] J.-C. Wang, L. Zhang, W.-X. Fang, J. Ren, Y.-Y. Li, H.-C. Yao, J.-S. Wang, Z.-J. Li, Enhanced photoreduction CO_2 activity over direct Z-scheme α-Fe_2O_3/Cu_2O heterostructures under visible light irradiation, ACS Appl. Mater. Interfaces 7 (2015) 8631–8639.
[11] J. Han, X. Zong, X. Zhou, C. Li, Cu_2O/CuO photocathode with improved stability for photoelectrochemical water reduction, RSC Adv. 5 (2015) 10790–10794.
[12] X.-M. Xiang, L. Zhang, L. Chou, X.-H. Li, Morphology-selective crystallization of cocatalysts on cuprous oxide with improved photocatalytic activity, CrystEngComm 16 (2014) 5180–5183.
[13] M. Schreier, J. Luo, P. Gao, T. Moehl, M.T. Mayer, M. Grätzel, Covalent immobilization of a molecular catalyst on Cu_2O photocathodes for CO_2 reduction, J. Am. Chem. Soc. 138 (2016) 1938–1946.
[14] K. Yao, X. Yin, T. Wang, H. Zeng, Synthesis self-assembly, disassembly, and reassembly of two types of Cu_2O nanocrystals unifaceted with {001} or {110} planes, J. Am. Chem. Soc. 132 (2010) 6131–6144.
[15] D. Jiang, W. Zhou, X. Zhong, Y. Zhang, X. Li, Distinguishing localized surface plasmon resonance and schottky junction of Au–Cu_2O composites by their molecular spacer dependence, ACS Appl. Mater. Interfaces 6 (2014) 10958–10962.
[16] C.-H. Kuo, Y.-C. Yang, S. Gwo, M.H. Huang, Facet-dependent and Au nanocrystal-enhanced electrical and photocatalytic properties of Au-Cu_2O core-shell heterostructures, J. Am. Chem. Soc. 133 (2011) 1052–1057.
[17] L. Li, X. Chen, Y. Wu, D. Wang, Q. Peng, G. Zhou, Y. Li, Pd-Cu_2O and Ag-Cu_2O hybrid concave nanomaterials for an effective synergistic catalyst, Angew. Chem. Int. Ed. 125 (2013) 11255–11259.
[18] X. Liang, L. Gao, S. Yang, J. Sun, Facile synthesis and shape evolution of single-crystal cuprous oxide, Adv. Mater. 21 (2009) 2068–2071.
[19] K. Chen, D. Xue, pH-assisted crystallization of Cu_2O: chemical reactions control the evolution from nanowires to polyhedra, CrystEngComm 14 (2012) 8068–8075.
[20] K. Nakaoka, J. Ueyama, K. Ogura, Photoelectrochemical behavior of electrodeposited CuO and Cu_2O thin films on conducting substrates, J. Electrochem. Soc. 151 (2004) C661–665.
[21] C. Morales-Guio, L. Liardet, M.T. Mayer, S.D. Tilley, M. Grätzel, X. Hu, Photoelectrochemical hydrogen production in alkaline solutions using Cu_2O coated with earth-abundant hydrogen evolution catalysts, Angew. Chem. Int. Ed. 54 (2015) 664–667.
[22] A. Tomizuka, H. Iwanaga, N. Shibata, Morphology and rotation twin of CuCl and CuBr crystals, J. Cryst. Growth 91 (1988) 27–32.
[23] A. Yanase, Y. Segawa, Nucleation and morphology evolution in the epitaxial growth of CuCl on MgO (001) and CaF_2 (111), Surf. Sci. 357 (1996) 885–890.